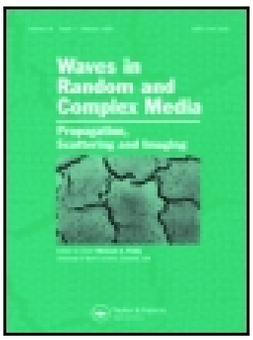

Waves in Random and Complex Media

ISSN: 1745-5030 (Print) 1745-5049 (Online) Journal homepage: http://www.tandfonline.com/loi/twrm20

Frequency domain finite-element and spectral-element acoustic wave modeling using absorbing boundaries and perfectly matched layer

Amin Rahimi Dalkhani, Abdolrahim Javaherian & Hadi Mahdavi Basir

To cite this article: Amin Rahimi Dalkhani, Abdolrahim Javaherian & Hadi Mahdavi Basir (2017): Frequency domain finite-element and spectral-element acoustic wave modeling using absorbing boundaries and perfectly matched layer, Waves in Random and Complex Media, DOI: 10.1080/17455030.2017.1355079

To link to this article: http://dx.doi.org/10.1080/17455030.2017.1355079

Published online: 24 Jul 2017.

WAVES IN RANDOM AND COMPLEX MEDIA, 2017
https://doi.org/10.1080/17455030.2017.1355079

Taylor & Francis
Taylor & Francis Group

Frequency domain finite-element and spectral-element acoustic wave modeling using absorbing boundaries and perfectly matched layer

Amin Rahimi Dalkhani[a], Abdolrahim Javaherian[a,b] and Hadi Mahdavi Basir[a]

[a]Department of Petroleum Engineering, Amirkabir University of Technology, Tehran, Iran; [b]Formerly Institute of Geophysics, University of Tehran, Tehran, Iran

ABSTRACT

Wave propagation modeling as a vital tool in seismology can be done via several different numerical methods among them are finite-difference, finite-element, and spectral-element methods (FDM, FEM and SEM). Some advanced applications in seismic exploration benefit the frequency domain modeling. Regarding flexibility in complex geological models and dealing with the free surface boundary condition, we studied the frequency domain acoustic wave equation using FEM and SEM. The results demonstrated that the frequency domain FEM and SEM have a good accuracy and numerical efficiency with the second order interpolation polynomials. Furthermore, we developed the second order Clayton and Engquist absorbing boundary condition (CE-ABC2) and compared it with the perfectly matched layer (PML) for the frequency domain FEM and SEM. In spite of PML method, CE-ABC2 does not add any additional computational cost to the modeling except assembling boundary matrices. As a result, considering CE-ABC2 is more efficient than PML for the frequency domain acoustic wave propagation modeling especially when computational cost is high and high-level absorbing performance is unnecessary.

ARTICLE HISTORY
Received 26 November 2016
Accepted 21 June 2017

1. Introduction

Wave propagation modeling can be conducted in both time domain and frequency domain, each of which has its advantages. Forward modeling methods in the frequency-space domain have many benefits: (1) They may simulate wave propagation from multiple sources at the same time, (2) interesting frequencies can be flexibly chosen, (3) wave propagation of each frequency can be independently computed, hence parallel computing can be carried out, (4) there are no accumulative errors, hence no stability problems, and (5) they are more suitable for viscous media than the time domain [1,2]. Therefore, certain advanced applications such as full waveform inversion can be applied more efficiently in the frequency domain [3–5].

CONTACT Abdolrahim Javaherian javaherian@aut.ac.ir

To date, several different methods have been employed for numerical wave propagation modeling including the finite-difference methods (FDM) [6–8], finite-element method (FEM) [9,10] and spectral-element method (SEM) [11]. Among the different methods, finite-element and spectral-element have the advantage of being flexible in dealing with complex geometry, which is applicable in the case of rug topography. The standard form of the FEM is rarely used in the time domain seismic wave propagation modeling due to the high computational cost and numerical dispersion [9,12,13]. Unlike the FEM in the time domain, it is computationally efficient in the frequency domain [14,15].

All numerical methods of wave propagation modeling suffer from the problem of artificial reflections from boundaries introduced by a truncated computational domain. A variety of methods has been proposed to truncate a model while emulating it as being infinite. All the methods can be categorized in three main groups of the absorbing boundary, absorbing layer and hybrid. The absorbing boundary methods are trying to suppress spurious reflections in truncation point and are based on approximations of the one-way wave equation. The methods proposed by Clayton and Engquist [16], Reynolds [17] and Higdon [18,19] are the main absorbing boundary methods. Collino used auxiliary variables to avoid computation of high derivatives in Higdon method and is known as high order absorbing boundary condition (ABC) [20]. This method then discussed and implemented by several researchers such as [21–23]. The absorbing layer methods are introducing an extra boundary layer to the modeling domain and are trying to gradually suppress wave amplitude in this layer. The sponge boundary layer [24–26] and perfectly matched layer (PML) [27–30] are the main methods of absorbing layers. The hybrid methods are trying to combine absorbing boundary methods and absorbing layer methods by introducing a transition zone to create a smooth transition between the one-way and two-way wave equations [31–33]. Recently, a new method proposed by [34] as the double ABC used in seismic modeling by [35]. It uses Collino method on two parallel artificial boundaries. The auxiliary variables are defined on the two boundaries and inside the layer bounded by them [34], so it is an absorbing layer that uses high order ABCs.

Each of the mentioned absorbing methods has its disadvantages. Clayton and Engquist absorbing boundary condition (CE-ABC), Higdon and Collino cannot readily treat corners in the finite-difference modeling. The sponge layer method seems not to be effective especially at absorbing low-frequency signals [35]. The PML method suffers from (1) instability in tangential incident waves, (2) complex theoretical derivations, (3) choosing proper parameters by trial and error, and (4) high computation cost [34,35]. The instability problems in PML can be avoided by the convolutional PML but at a high computation cost [36]. In the high-accuracy regime, the high order ABCs and the PML are equally effective [37].

In the case of high computational cost and unnecessary high-level absorbing performance such as migration and migration velocity analyses, high order ABCs are more preferable than boundary layer methods. The CE-ABC is a special case of the Higdon boundary but has difficulty in dealing with the corner points in finite-difference implementation and suffers from instability in the time domain modeling, especially for long-time modeling [38]. This method can be applied in the frequency domain FEM and SEM without any difficulty in dealing with the corner points and also without increasing computation cost of modeling. Also, frequency domain methods are unconditionally stable. Regarding the high computation cost of other methods in the frequency domain and sufficient accuracy of the second order CE-ABC2 for incident angles less than 45° (3% of the amplitude of the incident wave [39]), we chose it to perform in the frequency domain FEM and SEM. Hence, in the present

study, we performed the CE-ABC2 to the frequency domain FEM and SEM. We also implemented the PML method in the frequency domain SEM and compared it with the CE-ABC2. We discussed the CE-ABC performance and frequency domain aspects of FEM and SEM via numerical examples of a homogeneous model, a two-layer model, an anticline with considering topography, and a reverse fault derived from EAGE/SEG fault model.

2. Frequency domain FEM and SEM

2.1. Governing equations

The strong form of the frequency domain acoustic wave equation in a homogeneous medium is given by [2]:

$$-\omega^2 P(\omega) - c^2 \nabla^2 P(\omega) = f(\omega) \tag{1}$$

where P is the pressure wavefield, ω is the angular frequency, and c is the propagation velocity. The weak form of Equation (1) is as follows:

$$-\omega^2 \oint_{\Omega} P(\delta P)\mathrm{d}\Omega + \oint_{\Omega} c^2(\nabla P.\nabla \delta P)\mathrm{d}\Omega - \oint_{\Gamma} c^2(\nabla P.\boldsymbol{n})(\delta P)\mathrm{d}\Gamma = \oint_{\Omega} f(\delta P)\mathrm{d}\Omega \tag{2}$$

where Ω represents the region domain, that can be 2D or 3D, Γ represents the region boundary, δ is the variation operator, and $\boldsymbol{n}$ is the unit normal vector. The four terms in Equation (2) are mass, stiffness, boundary, and source terms, respectively. Equations (1) and (2) simulate a pure pressure wave propagating through region Ω with only a single component P representing the pressure wavefield in the medium at point x and time t.

Several different methods are available for the numerical modeling of acoustic wave propagation such as FDM, FEM and SEM. For all the differences in the technical details of the numerical methods, they have one point in common: They spatially discretize the propagation medium and approximate seismic response at different nodes. In all numerical methods, following spatial discretization, Equations (1) and (2) would be converted as follows:

$$-\omega^2 \mathbf{M}\boldsymbol{q}(\omega) + i\omega \mathbf{A}\boldsymbol{q}(\omega) + \mathbf{K}\boldsymbol{q}(\omega) = \boldsymbol{s}(\omega), \tag{3}$$

where $i = \sqrt{-1}$, $\mathbf{M}$, $\mathbf{A}$ and $\mathbf{K}$ are the mass, damping and stiffness matrices of the desired model, respectively, $\boldsymbol{q}$ and $\boldsymbol{s}$ are the column vectors of nodal pressure and external forces, respectively. The damping matrix $\mathbf{A}$ can be ignored if the medium is considered nonviscous; by considering the ABCs, however, the damping matrix $\mathbf{A}$ might appear. Equation (3) can be written as a linear system as:

$$\mathbf{B}(\omega)\boldsymbol{q}(\omega) = \boldsymbol{s}(\omega), \tag{4}$$

where $\mathbf{B}$ is the impedance matrix and can be written as:

$$\mathbf{B}(\omega) = -\omega^2 \mathbf{M} + i\omega \mathbf{A} + \mathbf{K}. \tag{5}$$

The solution of this equation is the discrete wavefield $\boldsymbol{q}$ at one frequency, ω. After solving this linear system for all the desired frequencies, the time domain response can be obtained by the inverse Fourier transform.

2.2. Spatial discretization

In elemental base methods, the complex geometry of the problem is divided into several smaller and simple elements for each of which, the integrals are calculated. In FEMs, the model responses within each element are achieved by the interpolation of the nodal Lagrange polynomials values. Therefore:

$$P = \sum_{i=1}^{n} N_i p_i, \tag{6}$$

where n is the number of nodes per element, N_i are the interpolation or element shape functions of the corresponding node and p_i are the nodal values of the model response (pressure). Here, the unknowns of the problem are the response of each node (p_i). Equation (6) can be expressed as the following matrix multiplication:

$$P = \boldsymbol{N}\boldsymbol{q_e}, \tag{7}$$

where

$$\boldsymbol{N} = \begin{bmatrix} N_1 & N_2 & \cdots & N_n \end{bmatrix}, \quad \boldsymbol{q_e} = \begin{bmatrix} p_1 \\ p_2 \\ \vdots \\ p_n \end{bmatrix}.$$

The variation of P can be written as follows:

$$\delta P = \boldsymbol{N}\delta\boldsymbol{q_e}. \tag{8}$$

Each term of Equation (2) can be discretized through the use of Equations (7) and (8). Following discretization, the element stiffness and mass matrices can be written as:

$$\mathbf{K}_e = \oint_{\Omega_k} c^2 \left(\boldsymbol{N}_x^T \boldsymbol{N}_x + \boldsymbol{N}_y^T \boldsymbol{N}_y + \boldsymbol{N}_z^T \boldsymbol{N}_z \right) \mathrm{d}\Omega, \tag{9}$$

where

$$\boldsymbol{N}_\alpha = \frac{\partial}{\partial \alpha}\boldsymbol{N},\ \boldsymbol{N}_a^T \text{ is the transpose of } \boldsymbol{N}_\alpha,\ \alpha \in \{x, y, z\}$$

$$\mathbf{M}_e = \oint_{\Omega_k} \boldsymbol{N}^T \boldsymbol{N} \mathrm{d}\Omega, \tag{10}$$

where $\mathbf{K}_e$, $\mathbf{M}_e$, and $\boldsymbol{N}$ are the element stiffness matrix, element mass matrix and element shape functions row vector, respectively. In the case of 2D (x–z plane), the $\boldsymbol{N}_y^T \boldsymbol{N}_y$ term in Equation (9) is omitted. $\mathbf{M}$ and $\mathbf{K}$ in Equation (3) are the total mass and stiffness matrices that are assembled from $\mathbf{K}_e$ and $\mathbf{M}_e$ from Equations (9) and (10).

So far, all the mentioned relationships, Equations (2)–(10), are identical for both finite-element and spectral-element methods. Differences between these two methods arise when choosing the interpolation points and numerical integration method. In the FEM, equispaced

nodal points are used. The spectral-element method is a higher-order FEM employing Gauss–Lobatto–Legendre (GLL) nodal points for interpolation functions. Another difference between FEM and SEM is in the numerical integration quadrature. In FEM, Gaussian quadrature is used while SEM makes use of GLL quadrature [11]. Employing GLL nodal points and GLL quadrature for the numerical integration, the mass matrix (Equation (10)) becomes single diagonal due to the orthogonality of Lagrange polynomials that leads to a high numerical efficiency of SEM in the time domain modeling.

3. Boundary condition

In seismic exploration, two main boundary conditions are implemented for wave modeling: free surface condition on the top side of the computational domain to represent the air–solid or air–water interfaces which have the highest impedance contrast, and ABCs to represent an infinite medium such as CE-ABC [16], sponge [24], and PML [27].

3.1. Free surface boundary condition

The pressure is zero at the free surface; thus, the boundary term in Equation (2) on the top of the model would be zero. In fact, the elemental base methods deal with free-surface boundary conditions naturally [40]. This flexibility in dealing with the free surface is one of the most superiority of elemental base methods in comparison with the finite difference method.

3.2. CE-ABC boundary conditions

So as to apply CE-ABC to FEM and SEM, we calculated the normal derivative of pressure on the boundaries, equivalent to $(\nabla P \cdot \boldsymbol{n})$ in the boundary term of Equation (2). In the case of the CE-ABC1, the normal derivative on the boundaries for all sides of a 2D model can be derived from the relationships proposed by [16] as follows:

$$\nabla P \cdot \boldsymbol{n} = -\frac{i\omega}{c} P. \tag{11}$$

By substituting this equation into the boundary term of Equation (2), one obtains

$$-\oint_{\Gamma} c^2 (\nabla P \cdot \boldsymbol{n})(\delta P) \mathrm{d}\Gamma = i\omega \oint_{\Gamma} c(\delta P)(P) \mathrm{d}\Gamma. \tag{12}$$

This equation can be discretized through the use of Equations (7) and (8). After finite-element discretization, the element damping matrix of absorbing boundaries can be written as follows:

$$\mathbf{A}_{eb}^{j} = \oint_{\Gamma_j} c \boldsymbol{N}^T \boldsymbol{N} \mathrm{d}\Gamma, \tag{13}$$

where $\mathbf{A}_{eb}^{j}$ is the damping matrix for the jth element on the boundary. This matrix is assembled in the total damping matrix $\mathbf{A}$ in Equation (3). Equation (13) is identical on all sides of

the model for the 2D and 3D cases, as well. It should be noted that unlike FDM, there is no need to solve extra equations for the corners of the model. The impedance matrix in the case of the CE-ABC1 is:

$$\mathbf{B}(\omega) = -\omega^2\mathbf{M} + i\omega\mathbf{Ab} + \mathbf{K}, \tag{14}$$

where $\mathbf{Ab}$ is the total damping matrix of the absorbing boundaries. The CE-ABC2 can be applied to the frequency domain the same as the CE-ABC1. In the case of the CE-ABC2, the normal derivative on the boundaries for the top and the bottom sides of a 2D model can be derived from the equations proposed by [16] as follows:

$$\nabla P \cdot \boldsymbol{n} = -\frac{i\omega}{c}P + \frac{c}{2i\omega}P_{xx}. \tag{15}$$

Moreover, for the left and the right sides of the model:

$$\nabla P \cdot \boldsymbol{n} = -\frac{i\omega}{c}P + \frac{c}{2i\omega}P_{zz}. \tag{16}$$

By substituting Equation (15) in the boundary term of Equation (2):

$$-\oint_{\Gamma} c^2(\nabla P.\boldsymbol{n})(\delta P)\mathrm{d}\Gamma = i\omega\oint_{\Gamma} c(\delta P)P\mathrm{d}\Gamma - \frac{1}{2i\omega}\oint_{\Gamma} c^3(\delta P)\left(P_{zz}\right)\mathrm{d}\Gamma. \tag{17}$$

The first term of Equation (17) is the same as that of Equation (12) hence, the element damping matrix is similar to the CE-ABC1 case and can be computed by Equation (13). The second term of Equation (17), using by-part integration, can be written as follows:

$$-\frac{1}{2i\omega}\oint_{\Gamma} c^3(\delta P)\left(P_{zz}\right)\mathrm{d}\Gamma = \oint_{\Gamma}\frac{c^3}{2i\omega}\left(\delta P_z\right)\left(P_z\right)d\Gamma - \frac{c^3}{2i\omega}(\delta P)\left(P_z\right)\Big|_{\Gamma_0}^{\Gamma_{\text{end}}}. \tag{18}$$

Following finite-element discretization via Equations (7) and (8), the stiffness matrix of absorbing boundaries for the jth element on the top and the bottom boundaries can be written as follows:

$$\mathbf{K}_{eb}^{j} = \oint_{\Gamma_j} c^3\boldsymbol{N}_x^T\boldsymbol{N}_x\mathrm{d}\Gamma - c^3\left(\boldsymbol{N}^T\boldsymbol{N}_x\right)\Big|_{x_0}^{x_{\text{end}}}. \tag{19}$$

Moreover, for the left and right boundaries we have:

$$\mathbf{K}_{eb}^{j} = \oint_{\Gamma_j} c^3\boldsymbol{N}_z^T\boldsymbol{N}_z\mathrm{d}\Gamma - c^3\left(\boldsymbol{N}^T\boldsymbol{N}_z\right)\Big|_{z_0}^{z_{\text{end}}}, \tag{20}$$

where x_0 and z_0 are the start points of each element and x_{end}, z_{end} are the end points of each element; the second term has to be calculated at these points. The impedance matrix in the case of the CE-ABC2 is:

$$\mathbf{B}(\omega) = -\omega^2\mathbf{M} + i\omega\mathbf{Ab} + \frac{1}{2i\omega}\mathbf{Kb} + \mathbf{K}, \tag{21}$$

where $\mathbf{Ab}$ and $\mathbf{Kb}$ are the total boundary damping and stiffness matrices obtained from Equations (13), (19) and (20) for the elements of absorbing boundaries.

3.3. Perfectly matched layer

To compare the CE-ABC2 with the PML, we used the method proposed by [28,41]. This PML technique can be obtained by incorporating the damping functions d_x and d_z into Equation (1) as follows:

$$-\omega^2 P - c^2\left(\frac{1}{d_x}\frac{\partial}{\partial x}\left(\frac{1}{d_x}\frac{\partial P}{\partial x}\right) + \frac{1}{d_z}\frac{\partial}{\partial z}\left(\frac{1}{d_z}\frac{\partial P}{\partial z}\right)\right) = f, \tag{22}$$

where

$$d_x = 1 - \frac{i}{\omega}d_0\left(\frac{x_i}{L_{\text{pml}}}\right)^2, \quad d_z = 1 - \frac{i}{\omega}d_0\left(\frac{z_i}{L_{\text{pml}}}\right)^2, \text{ and } d_0 = \frac{3Vp_{\max}}{2L_{\text{pml}}}\log\left(\frac{1}{R}\right),$$

$Vp_{\max}$ is the maximum of the P-wave velocity, R is the theoretical reflection coefficient, L_{pml} is the width of PML layer, x_i and z_i are locations of grid points in the PML layer varying from zero at the inner border of the PML layer to L_{pml} at the outer border of the PML layer in the x- and z-directions, respectively. The absorption efficiency of the PML mostly depends on the width of the PML layer and the chosen coefficient R [33,41]. After finite-element discretization, the frequency dependent element stiffness matrix for the jth element on the PML layer can be written as follows:

$$\mathbf{K}^j_{\text{epml}} = \oint c^2\left(\frac{1}{d_x^2}\boldsymbol{N}_x^T\boldsymbol{N}_x - \frac{1}{d_x^3}\left(\frac{\partial d_x}{\partial x}\right)\boldsymbol{N}^T\boldsymbol{N}_x + \frac{1}{d_z^2}\boldsymbol{N}_z^T\boldsymbol{N}_z - \frac{1}{d_z^3}\left(\frac{\partial d_z}{\partial z}\right)\boldsymbol{N}^T\boldsymbol{N}_z\right)\mathrm{d}\Omega^j. \tag{23}$$

Then the impedance matrix in the case of PML can be written as follows:

$$\mathbf{B}(\omega) = -\omega^2\mathbf{M} + \mathbf{K} + \mathbf{K}_{\text{pml}}(\omega), \tag{24}$$

where $\mathbf{K}_{\text{pml}}$ is the total PML stiffness matrix obtained by assembling Equation (23) for all elements of the PML layer. The procedure for implementing CE-ABC1, CE-ABC2 and PML methods in the frequency domain FEM and SEM are depicted in Figure 1. It can be seen that in the PML method, the PML stiffness matrix is frequency dependent and must be recalculated and reassembled in each frequency step that will increase computation time and cost (CPU time) of the frequency domain modeling.

4. Practical aspects and numerical efficiency

In the time domain modeling, two parameters are to be adjusted: time step length (Δt) for numerical stability and spatial step length (Δx) for numerical dispersion. In addition to Δx, the frequency step length (Δf) must be adjusted in the frequency domain modeling in order to minimize the time aliasing.

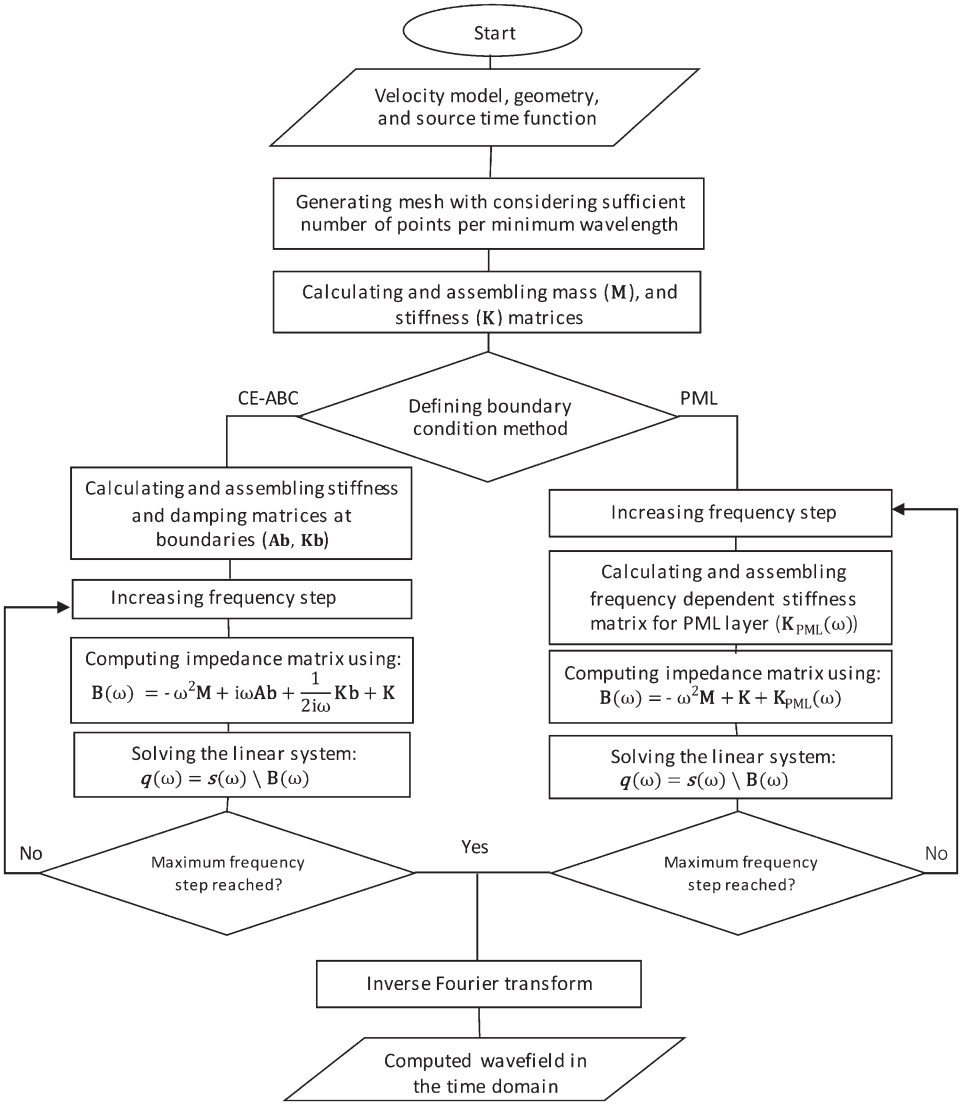

Figure 1. Flowchart for frequency domain acoustic wave modeling using FEM and SEM with considering CE-ABC or PML boundary conditions.

4.1. Time aliasing

The frequency domain is unconditionally stable yet is influenced by the time aliasing. To reduce this effect, Δf has to be sufficiently small, but decreasing Δf means that $P(\omega)$ must be computed at more points requiring a great deal of computational cost and run time. Mallik and Frazer employed a complex frequency technique for anti-aliasing [42]. The so-called frequency shift property of Fourier transform states that:

$$P(\omega - ia) \leftrightarrow e^{-at}P(t), \tag{25}$$

where $i = \sqrt{-1}$ and a is a small positive constant meaning that by computing $P(\omega - ia)$ in the frequency domain, the time response of the model is multiplied by a descending exponential function (e^{-at}). This multiplication exponentially decays pressure amplitude by increasing time. So, the amplitude of the phenomena after t_{max} is attenuated by at least $e^{-at_{max}}$ in the frequency domain, and they cannot be transformed to the time domain by the inverse Fourier transform. To find the true amplitude of the model responses, the inversed Fourier transform must be subsequently multiplied by e^{at}. Hence, in complex frequency technique, instead of computing $P(\omega)$, $P(\omega - ia)$ is computed; the time response is then multiplied by e^{-at}.

4.2. Numerical dispersion and efficiency

For Δx, we are to consider approximately 10 nodes per minimum wavelength in the second order standard grid FDM [43,44], FEM with linear interpolation polynomials [44] and 4.5 nodes per minimum wavelength in SEM with the fourth order interpolation polynomials [45,46]. Decreasing the number of nodes per minimum wavelength increases the numerical efficiency due to the reduction in the degrees of freedom related to the computational model, resulting in smaller matrices in the linear system of Equation (4).

Another parameter that affects the numerical efficiency in solving this linear system is the number of nonzero diagonals of the impedance matrix. If the number of nonzero diagonals increases, the computational time and cost will significantly increase. Table 1 shows the number of the nonzero diagonals of impedance matrix in SEM and FEM with different orders of interpolation polynomials. Despite the accuracy of higher order SEM and its numerical efficiency in the time domain, it seems that using frequency domain SEM with higher order polynomials is costly and time-consuming. Employing SEM with order of polynomials more than 3 is not recommended in the frequency domain, because of substantial increase in the computational run time by the increase in the number of nonzero diagonals. The standard form of FEM is rarely used in the time domain seismic wave propagation because of its high numerical dispersion and high computational cost and run time; in the frequency domain, on the other hand, the computational cost and run time of FEM are the same as FDM and SEM. It seems that if the second order interpolation polynomials were to be employed, FEM would be efficient and accurate in the frequency domain, an issue further discussed in the numerical results and discussion.

5. Numerical results and discussion

In this section, four different 2D models were employed in order to investigate the performance of boundary conditions in the frequency domain using FEM and SEM. The first

Table 1. Number of nonzero diagonals of impedance matrix in the frequency domain FEM and SEM modeling of acoustic wave propagation.

Order of interpolation polynomials	2D FEM	2D SEM	3D FEM	3D SEM
1	9	5	27	7
2	25	9	125	13
3	49	49	343	127
4	81	81	729	217
5	121	121	1331	331
6	169	169	2197	469

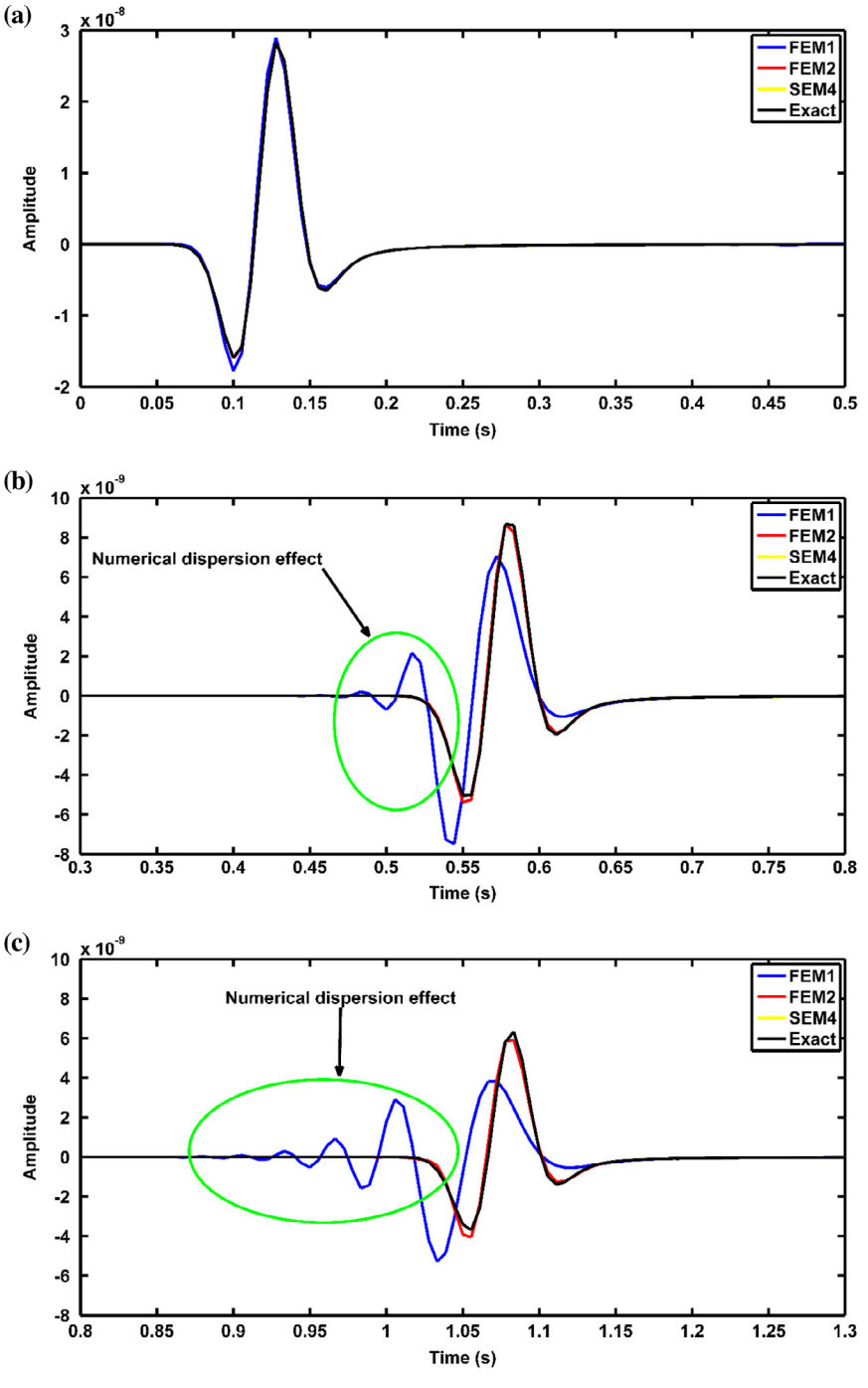

Figure 2. Numerical dispersion and accuracy of the frequency domain FEM and SEM modeling of acoustic wave propagation. (a–c) Responses of a simple homogeneous model with P-wave velocity of 2000 m/s at offsets of 90, 900, and 1800 m, respectively. The source is a Ricker wavelet of 20 Hz. FEM1, FEM2, SEM4 and Exact refer to the finite element using the first order interpolation polynomials, the finite element using the second order interpolation polynomials, the spectral element using the fourth order interpolation polynomials and the exact response of the model using Gar6more2D package.

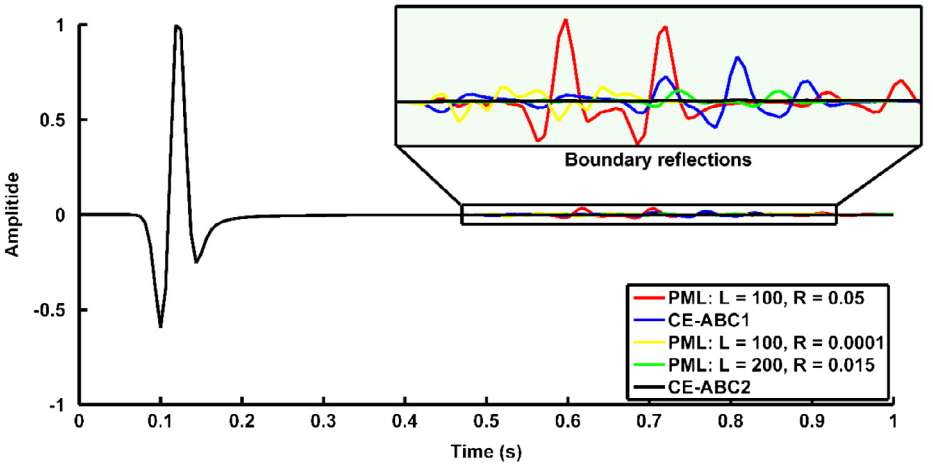

Figure 3. Comparison of the absorption efficiency of boundary condition methods in a 2D homogeneous acoustic medium using the frequency domain SEM. The model dimensions in the x- and z-directions are 1000 m (201 × 201 grid points) and the P-wave velocity of the medium is 2000 m/s. The source is located at the center of the model at $(x, z) = (500,\ 500)$. The receiver is located at $(x, z) = (600,\ 600)$. The source is a Ricker wavelet of 20 Hz.

example contains a 2D homogeneous model. In this example, the numerical dispersion and accuracy of frequency domain FEM and SEM, and the efficiency of CE-ABC boundary conditions in comparison with the PML layer are discussed using the trace response of certain points. In the second example, the PML method, the CE-ABC1 and the CE-ABC2 are compared using the shot records of a model containing horizontal layers. The third example contains a 2D anticline model with topography so as to evaluate the efficiency and accuracy of the frequency domain FEM and SEM acoustic wave modeling. The last example depicts a reverse fault in a rather large-scale model where the effect of the time aliasing is shown on a shot record. Zero-offset section was generated using the CE-ABC2. Modeling was performed using MATLAB software and a four-core machine with 6 GB of RAM.

5.1. Homogeneous model

Figure 2 shows the numerical dispersion and accuracy of FEM and SEM modeling of acoustic wave propagation. The responses of a simple homogeneous model are depicted at three different points far from the source point, using FEM with linear interpolation polynomials (FEM1), FEM with second order interpolation polynomial (FEM2), spectral-element using fourth order interpolation polynomials (SEM4) and the exact response of the model using Gar6more2Dpackage [47]. The number of grid points per minimum wavelength in FEM1, FEM2 and SEM4 are 7, 5.5 and 5, respectively. The computation times of FEM1, FEM2 and SEM4, in a 3000 m × 3000 m model, are 93, 102 and 215 s using a four-core machine, respectively. Figure 2 indicates that by moving away from the source, the numerical dispersion increases in FEM1. FEM2 is highly accurate and, like SEM4, has very little numerical dispersion. SEM, with second order interpolation polynomial (SEM2) and using 5–6 nodes per minimum wavelength, entailed results the same as FEM2. Owing to the impedance matrix with less nonzero diagonals, FEM2 and SEM2 are more numerically efficient than SEM4, yet need more

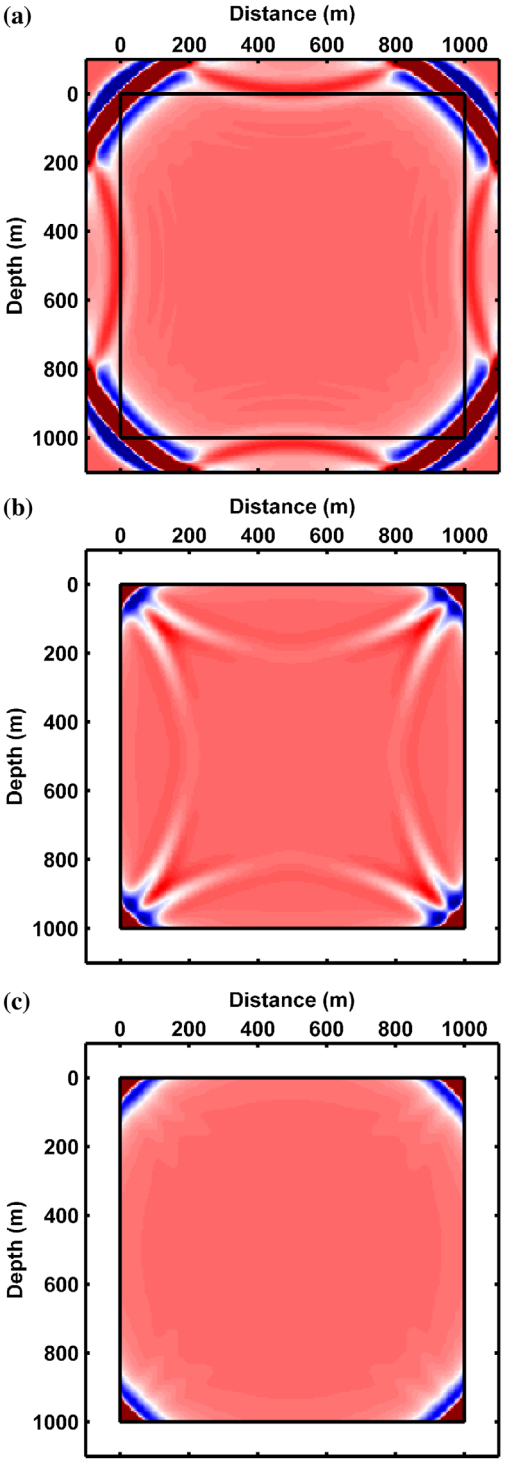

Figure 4. Snapshots of the 2D homogeneous model of Figure 3 using the frequency domain SEM with (a) PML100 considering $R = 0.05$, (b) CE-ABC1, and (c) CE-ABC2. To see boundary reflections, the results are magnified by a factor of 100.

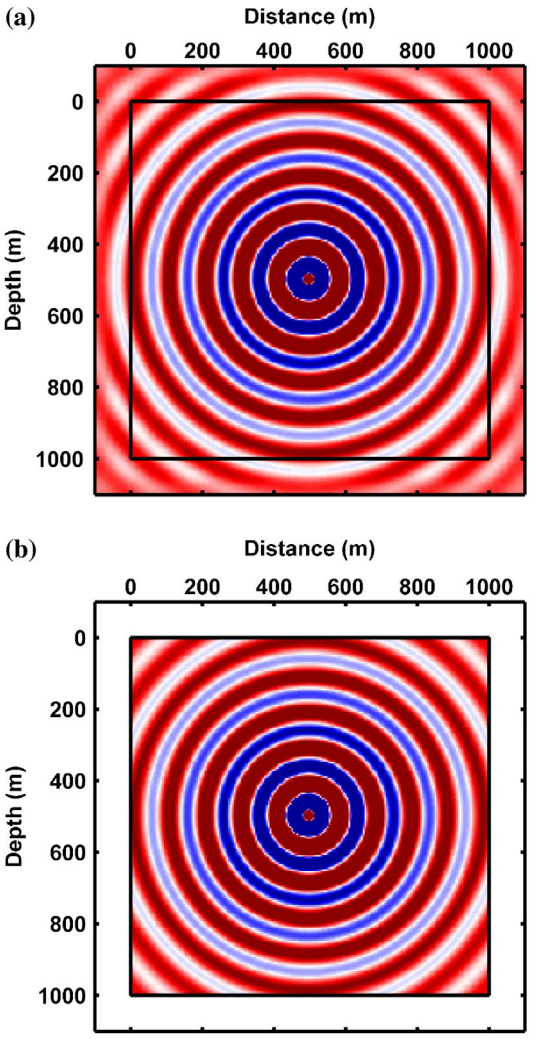

Figure 5. The 20-Hz real-part frequency response of the 2D homogeneous model of Figure 3 using SEM frequency domain modeling with (a) PML100 considering $R = 0.05$, and (b) CE-ABC2.

nodes per minimum wavelength than SEM4 so as to achieve a similar accuracy. Hence, FEM2 and SEM2 are accurate and efficient methods for wave propagation modeling in the frequency domain using 5–6 nodes per minimum wavelength. Figure 3 illustrates the acoustic responses of a 2D homogeneous medium using the PML with the width of 100 m and $R = 0.05$ & 0.0001 (PML100), CE-ABC1, PML with the width of 200 meter and $R = 0.015$ (PML200), and the CE-ABC2 with SEM frequency domain modeling. This figure shows the efficiency of CE-ABC2 over CE-ABC1 and PML. It is noteworthy that in the case of SEM and FEM using the first order or linear interpolation polynomials, K^{j}_{eb} (Equations (19) and (20)) is zero; accordingly, the CE-ABC1 and the CE-ABC2 have the same results. Hence, in order to apply the CE-ABC2, at least the second order interpolation polynomial is necessary. The time domain snapshot and the real-part frequency domain solution for the homogeneous acoustic medium with PML100, CE-ABC1, and CE-ABC2 are depicted in Figures 4 and 5. To see boundary reflections,

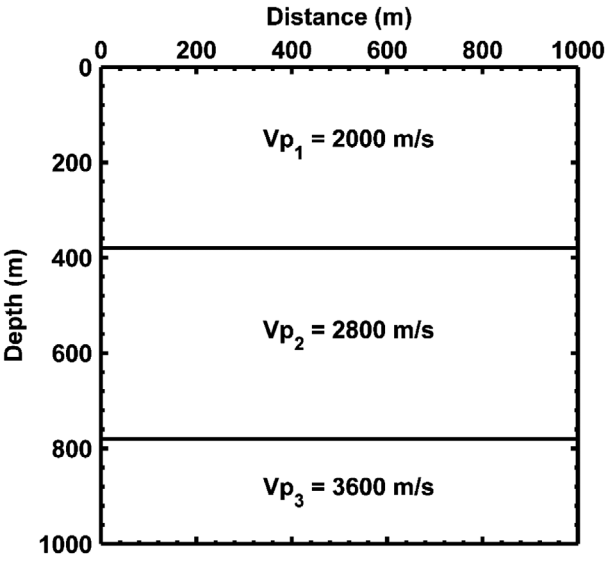

Figure 6. A simple earth model for comparing different boundary conditions (PML100, PML200, and CE-ABC2) on a shot record.

the results are magnified by a factor of 100. The boundary reflections are very small in comparison with the incident wave and do not affect the frequency responses significantly. Hence, Figure 5 does not show a significant difference between the frequency results with different boundary conditions.

5.2. Two horizontal layers over a half space

Figure 6 depicts an earth model with two horizontal layers over a half-space. Figure 7 shows a shot record of the acoustic wave propagation of Figure 6 with the frequency domain SEM. The top of the model is considered as the free surface boundary condition. The other sides of the model are considered as PML100 in Figure 7(a), PML200 in Figure 7(b), and CE-ABC2 in Figure 7(c). The computation time of modeling using the four-core machine is presented in Figure 7(d). Different events are specified and spurious boundary reflections significantly decreased in Figures 7(b)–(c) by using PML200 and CE-ABC2. However, the boundary reflections by CE-ABC2 are weaker with significantly lower computational cost than those by PML200 (Figure 7(d)).

5.3. Anticline model with topography

This example contains a simple anticline model with a smooth topography (Figure 8). Modeling is done with the frequency domain SEM2. The multi-source modeling is performed with 105 source points on the top of the model in order to generate zero-offset sections of Figure 9. The boundary condition for the top of the model is the free surface and boundary condition for the other sides of the model is PML100 with $R = 0.015$ in Figure 9(a), and CE-ABC2 in Figures 9(b)–(d). The maximum time of modeling is 2 s and a Ricker wavelet with a peak frequency of 15 Hz is used as the source. The modeling is performed for 120 frequency

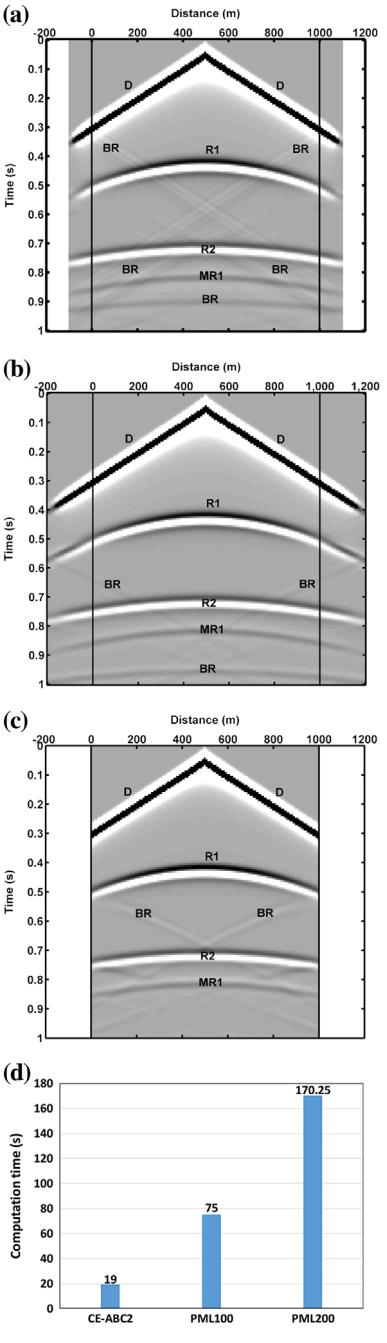

Figure 7. Shot records of acoustic wave propagation in Figure 6 using the frequency domain SEM with (a) PML100 considering $R = 0.015$, (b) PML200 considering $R = 0.05$, (c) CE-ABC2. D, R1, R2, MR1, and BR are the direct wave, the reflection from the first interface, the reflection from the second interface, the first order multiple from the first interface, and the spurious boundary reflections, respectively. Boundary condition at the top of the model is considered as the free surface. The source is a Ricker wavelet of 20 Hz. The model in the x- and z-directions are discretized by 201×201 grid points. To see boundary reflections, the results are magnified by a factor of 100. (d) Computation time of modeling using a 4 core machine for CE-ABC2, PML100, and PML200.

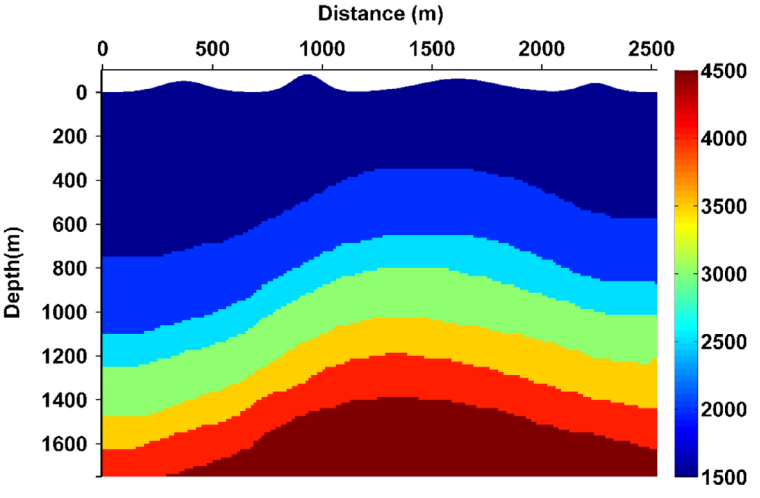

Figure 8. A simple anticline model with a smooth topography for comparing PML100 and CE-ABC2 on zero-offset sections.

components up to 60 Hz. The minimum P-wave velocity in the model is 1500 m/s. Spatial discretization is conducted with 6 nodes per minimum wavelength, hence the grid point interval is 6.25 m and the vertical and the horizontal dimensions of the model are 281×417 grid points, respectively. Employing the four-core machine and MATLAB software, the CPU times needed to perform modeling using CE-ABC2 are 2 min and 3 h in single-source and multi-source cases, respectively. The CPU times needed to perform modeling using PML100 is 4.3 min and 6.7 h in single-source and multi-source cases, respectively. It must be noted that recalculating and assembling stiffness matrix for the PML layer at each frequency step is a very time-consuming task in MATLAB [4]. To increase PML computation efficiency, we performed this part of computer program code using a C++ compiler by building a MEX file in MATLAB. The computation time for the multi-source case considering PML100 was 28 h before using the C++ compiler.

Figures 9(a)–(b) state that CE-ABC2 does not perform better than PML100 near boundaries or for high incident angles. However, the computation cost of PML is significantly high and also the performance of CE-ABC2 for lower incident angles is significantly better than PML. To avoid low efficiency of CE-ABC2 in high incident angles, it is more efficient to consider a 200 m layer around the model and use CE-ABC2 at the outer borders of the model instead of using PML layer with the width of 100 m. In addition, PML method suffers from choosing proper parameters by trial and error. Figure 9(c) shows the zero-offset section of multi-source modeling by considering CE-ABC2 at 200 m far from the right and left sides of the model. The CPU time for multi-source modeling, in this case, was 4 h that is significantly lower than considering PML100.

In Figure 9(d) the result of frequency domain SEM2 with CE-ABC2 by removing the surface topography of Figure 8 is presented. This figure shows the effect of surface topography in real cases on the modeling results, the ability of SEM in dealing with surface topography, and applying free surface boundary condition especially for the models with surface topography. Finally, it indicates that the second order SEM using 6 nodes per minimum wavelength

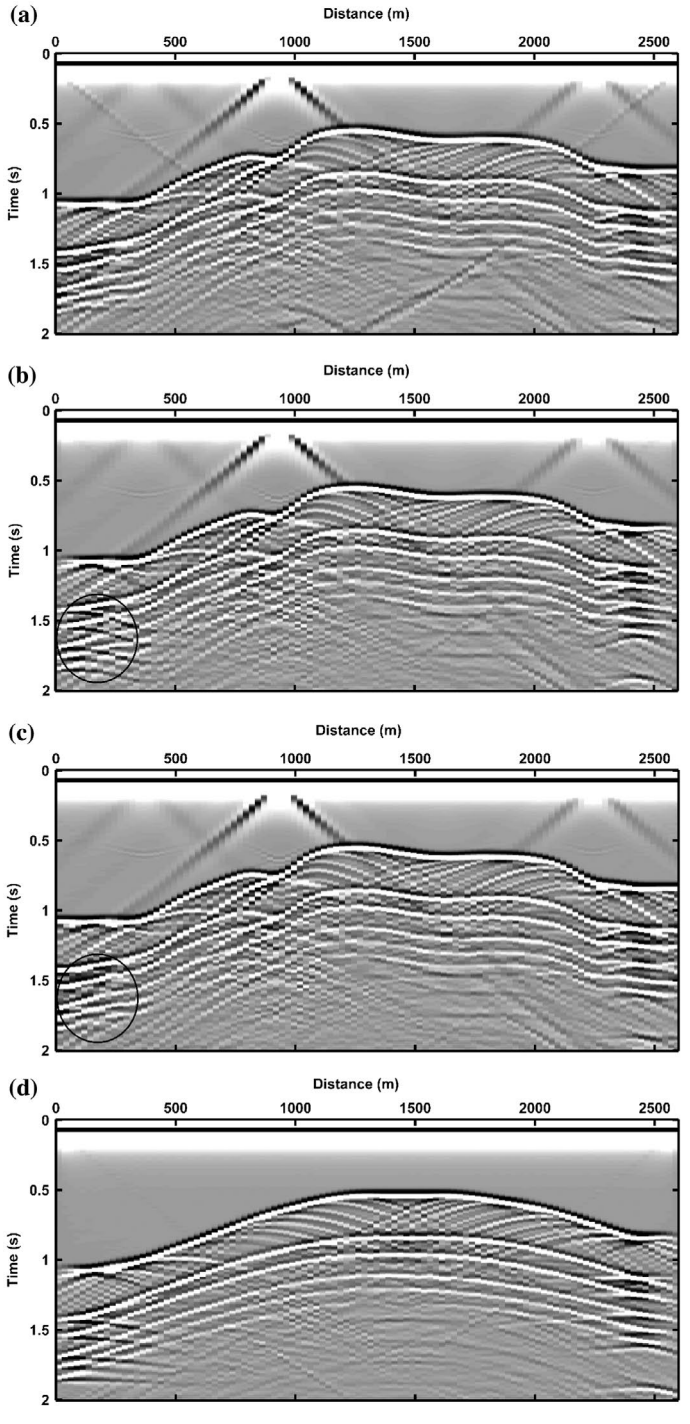

Figure 9. Zero-offset sections of Figure 8 using frequency domain FEM with the second order interpolation polynomials with (a) PML100 considering $R = 0.015$, (b) CE-ABC2, and (c) considering CE-ABC2 at 200 m far from the left and right sides of the model, and (d) CE-ABC2 with no topography. Circles in (b) and (c) show spurious boundary reflections. The boundary condition at the top of the model is considered as the free surface. To see the effect of the boundary reflections, the results are magnified by a factor of 100.

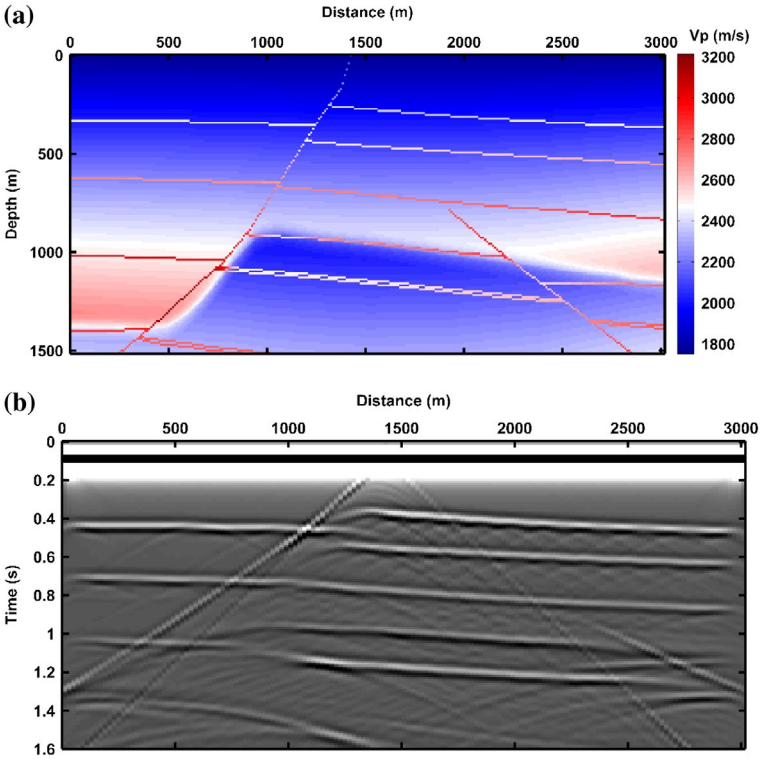

Figure 10. (a) A portion of the SEG\EAGE fault model [48], (b) Zero-offset section of (a) using frequency domain SEM with the second order interpolation polynomials. Boundary condition at the top of the model is considered as the free surface and the boundary condition for the other sides of the model is considered as CE-ABC2. The source-time function is a Ricker wavelet of 12 Hz. To see the spurious reflections from the boundaries, the results are magnified by a factor of 100.

and the CE-ABC2 have sufficient accuracy and efficiency in order to perform frequency domain acoustic wave propagation modeling in complex 2D media.

5.4. Reverse fault model

In this example, we considered a more realistic earth model, Figure 10(a). This model is a portion of the SEG\EAGE fault model obtained from the SEG/EAGE salt model [48]. Figure 10(b) is the zero-offset section of Figure 10(a) captured by receivers coincident with sources at the top of the model using frequency domain SEM2. The boundary condition at the top of the model is considered as the free surface and the boundary condition for the other sides of the model is considered as CE-ABC2. Maximum time of the modeling is 2 s and a Ricker wavelet with a peak frequency of 12 Hz is used as the source. The modeling is performed for 98 frequency components up to 48 Hz. The minimum P-wave velocity in the model is 1760 m/s. Spatial discretization is conducted with 5.5 nodes per minimum wavelength that led to an acceptable response. The grid point interval is 10 m and the vertical and the horizontal dimensions of the model are 151 $\times$ 303 grid points, respectively. Using MATLAB software and the four-core machine, the CPU times required to perform the modeling were

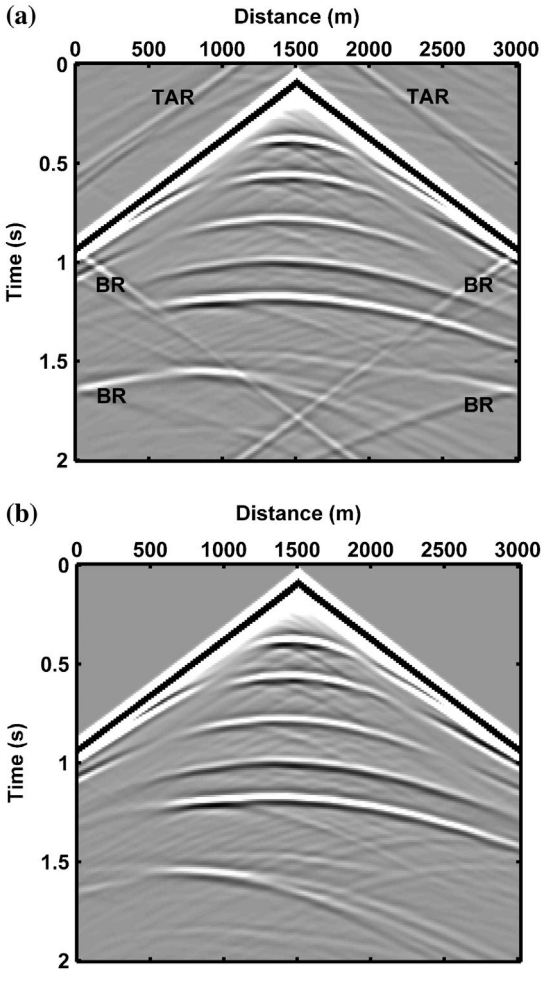

Figure 11. The effect of the time aliasing and absorbing boundary condition on a shot record of acoustic wave propagation in Figure 10 using the frequency domain SEM. (a) Without anti-time aliasing and considering CE-ABC1. TA and BR are time aliased and boundary reflections, respectively. (b) With anti-time aliasing and CE-ABC2. Spatial discretization is performed through 6 nodes per minimum wavelength. The source-time function is a Ricker wavelet of 12 Hz. Boundary condition at the top of the model is considered as the free surface. To see the spurious reflections from the boundaries, the results are magnified by a factor of 100.

about 40 s and 50 min in single-source and multi-source cases, respectively. The multi-source modeling is performed with 150 source points on top of the model so as to generate zero-offset section. Ultimately, it can be seen that SEM2 using 5–6 nodes per minimum wavelength and CE-ABC2 are sufficiently accurate and efficient to perform frequency domain acoustic wave propagation modeling in complex and random media.

Figure 11 shows the effect of time aliasing and ABCs on a shot record of Figure 10(a) using the frequency domain SEM. Figure 11(a) is a shot record of the model using the CE-ABC1 without the complex frequency technique whereas Figure 11(b) is a shot record of the model using CE-ABC2 and the complex frequency technique with much small spurious boundary reflections than Figure 11(a).

6. Conclusions

In this paper, frequency domain FEM and SEM were performed and evaluated for acoustic wave propagation modeling with consideration and comparison of CE-ABC1, CE-ABC2 and PML. The results demonstrated that the frequency domain SEM has a good accuracy and numerical efficiency with the second order interpolation polynomials. In spite of the accuracy of higher order SEM and its numerical efficiency in the time domain modeling, the frequency domain SEM using higher order polynomials leads to more computational cost and time. Moreover, in spite of high computational cost and high numerical dispersion of time domain FEM using the linear interpolation polynomials, with the use of the second order interpolation polynomials, FEM is efficient in the frequency domain modeling. In the other hand, CE-ABC1, CE-ABC2 and PML were applied to the frequency domain modeling by evaluating their absorbing performance and numerical efficiency. The computation cost of PML is significantly high and also the performance of CE-ABC2 for lower incident angles is significantly better than PML. In addition, PML method suffers from choosing proper parameters. However, CE-ABC2 does not perform better than PML near boundaries or for high incident angles. To avoid low efficiency of CE-ABC2 in high incident angles, we considered a 200 m layer around the model and used CE-ABC2 at the outer borders of the model instead of using PML layer with the width of 100 m that led to more efficient results. Hence, in comparison with CE-ABC1 and PML, CE-ABC2 is more efficient and more applicable in frequency domain seismic exploration uses especially when modeling domain is very large and high-level absorbing performance is unnecessary.

Disclosure statement

No potential conflict of interest was reported by the authors.

References

[1] Liao J, Wang H, Ma Z. 2-D elastic wave modeling with frequency-space 25-point finite-difference operators. Appl Geophys. 2009;6:259–266.
[2] Fichtner A. Full seismic waveform modelling and inversion. Berlin: Springer; 2011.
[3] Hustedt B, Operto S, Virieux J. Mixed-grid and staggered-grid finite-difference methods for frequency-domain acoustic wave modelling. Geophys J Int. 2004;157:1269–1296.
[4] Amini N, Javaherian A. A MATLAB-based frequency-domain finite-difference package for solving 2D visco-acoustic wave equation. Waves Random Media. 2011;21:161–183.
[5] Zhang QJ, Dai SK, Chen LW, et al. Two-dimensional frequency-domain acoustic full-waveform inversion with rugged topography. Appl Geophys. 2015;12:378–388.
[6] Boore DM. Love waves in nonuniform wave guides: finite difference calculations. J Geophys Res. 1970;75:1512–1527.
[7] Boore DM. Finite difference methods for seismic wave propagation in heterogeneous materials. In: Bolt BA, editor. Methods in computational physics. New York (NY): Academic Press; 1972. p. 1–37.
[8] Virieux J. SH -wave propagation in heterogeneous media: velocity-stress finite-difference method. Geophysics. 1984;49:1933–1942.
[9] Lysmer J, Drake LA. A finite element method for seismology. In: Bolt BA, editor. Methods in computational physics. New York (NY): Academic Press; 1972. p. 181–216.
[10] Gan H, Levin P, Ludwig R. Finite element formulation of acoustic scattering phenomena with absorbing boundary condition in the frequency domain. J Acoust Soc Am. 1993;94:1651–1662.
[11] Komatitsch D, Tromp J. Introduction to the spectral element method for three-dimensional seismic wave propagation. Geophys J Int. 1999;139:806–822.

[12] Bao H, Bielak J, Ghattas O, et al. Large-scale simulation of elastic wave propagation in heterogeneous media on parallel computers. Comput Methods Appl Mech Eng. 1998;152:85–102.
[13] Harari I. A survey of finite element methods for time-harmonic acoustics. Comput Methods Appl Mech Eng. 2006;195:1594–1607.
[14] Marfurt K. Seismic modeling: A frequency-domain/finite-element approach. SEG Technical Program Expanded Abstracts; 1984;S15.6:633–634.
[15] Zhou B, Greenhalgh S. 3-D frequency-domain seismic wave modelling in heterogeneous, anisotropic media using a Gaussian quadrature grid approach. Geophys J Int. 2011;184:507–526.
[16] Clayton R, Engquist B. Absorbing boundary conditions for acoustic and elastic wave equations. Bull Seismol Soc Am. 1977;67:1529–1540.
[17] Reynolds AC. Boundary conditions for the numerical solution of wave propagation problems. Geophysics. 1978;43:1099–1110.
[18] Higdon RL. Absorbing boundary conditions for elastic waves. Geophysics. 1991;56:231–241.
[19] Higdon RL. Numerical absorbing boundary conditions for the wave equation. Math Comp. 1987;49:65–90.
[20] Collino F. High order absorbing boundary conditions for wave propagation models. Straight line boundary and corner cases. Proceedings of the Second International Conference on Mathematical and Numerical Aspects of Wave Propagation; 1993 Jun 7–10; Newark (DE).
[21] Hagstrom T, Warburton T. A new auxiliary variable formulation of high-order local radiation boundary conditions: corner compatibility conditions and extensions to first-order systems. Wave Motion. 2004;39:327–338.
[22] Givoli D. High-order local non-reflecting boundary conditions: a review. Wave Motion. 2004;39:319–326.
[23] Givoli D, Neta B. High-order non-reflecting boundary conditions for dispersive waves. Wave Motion. 2003;37:257–271.
[24] Cerjan C, Kosloff D, Kosloff R, et al. A nonreflecting boundary condition for discrete acoustic and elastic wave equations. Geophysics. 1985;50:705–708.
[25] Kosloff R, Kosloff D. Absorbing boundaries for wave propagation problems. J Comput Phys. 1986;63:363–376.
[26] Sochacki J, Kubichek R, George J, et al. Absorbing boundary conditions and surface waves. Geophysics. 1987;52:60–71.
[27] Berenger JP. A perfectly matched layer for the absorption of electromagnetic waves. J Comp Phys. 1994;114:185–200.
[28] Collino F, Tsogka C. Application of the perfectly matched absorbing layer model to the linear elastodynamic problem in anisotropic heterogeneous media. Geophysics. 2001;66:294–307.
[29] Komatitsch D, Martin R. An unsplit convolutional perfectly matched layer improved at grazing incidence for the seismic wave equation. Geophysics. 2007;72:SM155–SM167.
[30] Liu Y, Sen MK. A hybrid scheme for absorbing edge reflections in numerical modeling of wave propagation. Geophysics. 2010;75:A1–A6.
[31] Liu Y, Sen MK. A hybrid absorbing boundary condition for elastic staggered-grid modelling. Geophys Prospect. 2012;60:1114–1132.
[32] Jiang Z, Bancroft JC, Lines LR. Combining absorbing and nonreflecting boundary conditions for elastic wave simulation. CREWES Res Rep. 2009;21:1–6.
[33] Moreira RM, Cetale Santos MA, Martins JL, et al. Frequency-domain acoustic-wave modeling with hybrid absorbing boundary conditions. Geophysics. 2014;79:A39–A44.
[34] Hagstrom T, Givoli D, Rabinovich D, et al. The double absorbing boundary method. J Comput Phys. 2014;259:220–241.
[35] Liu Y, Li XY, Chen SQ. Application of the double absorbing boundary condition in seismic modeling. Appl Geophys. 2015;12:111–119.
[36] Roden JA, Gedney SD. Convolution PML (CPML): An efficient FDTD implementation of the CFS-PML for arbitrary media. Microw Opt Technol Lett. 2000;27:334–339.
[37] Rabinovich D, Givoli D, Bécache E. Comparison of high-order absorbing boundary conditions and perfectly matched layers in the frequency domain. Int J Numer Method Biomed Eng. 2010;26:1351–1369.

[38] Gao Y, Song H, Zhang J, et al. Comparison of artificial absorbing boundaries for acoustic wave equation modelling. Explor Geophys. 2015;48:76–93.
[39] Engquist B, Majda A. Absorbing boundary conditions for numerical simulation of waves. Proc Nat Acad Sci USA. 1977;74:1765–1766.
[40] Komatitsch D, Vilotte J-P. The spectral element method: an efficient tool to simulate the seismic response of 2D and 3D geological structures. Bull Seismol Soc Am. 1998;88:368–392.
[41] Ren Z, Liu Y. A hybrid absorbing boundary condition for frequency-domain finite-difference modelling. J Geophys Eng. 2013;10:054003.
[42] Mallick S, Frazer LN. Practical aspects of reflectivity modeling. Geophysics. 1987;52:1355–1364.
[43] Alford R, Kelly K, Boore DM. Accuracy of finite-difference modeling of the acoustic wave equation. Geophysics. 1974;39:834–842.
[44] Marfurt kJ. Accuracy of finite-difference and finite-element modeling of the scalar and elastic wave equations. Geophysics. 1984;49:533–549.
[45] Seriani G, Priolo E. Spectral element method for acoustic wave simulation in heterogeneous media. Finite Elem Anal Des. 1994;16:337–348.
[46] De Basabe JD, Sen MK. Grid dispersion and stability criteria of some common finite-element methods for acoustic and elastic wave equations. Geophysics. 2007;72:T81–T95.
[47] Diaz J, Ezziani A. Analytical solution for waves propagation in heterogeneous acoustic/porous media. Part I: the 2D case. Commun Comput Phys. 2010;7:171–194.
[48] Exercise in prestack migration under the Born approximation. 2009. Available from: https://utam.gg.utah.edu/Inter.LAB1/CH2.lab/lab.mig.pre/lab.html.